Polymer 50 (2009) 4935–4943

Contents lists available at ScienceDirect

Polymer

journal homepage: www.elsevier.com/locate/polymer

Scaling law on particle-to-fiber formation during electrospinning

Muhammad Miftahul Munir [a,b], Adi Bagus Suryamas [a], Ferry Iskandar [a], Kikuo Okuyama [a,*]

[a] Department of Chemical Engineering, Graduate School of Engineering, Hiroshima University, Higashi-hiroshima, Hiroshima 739-8527, Japan
[b] Department of Physics, Bandung Institute of Technology (ITB), Jalan Ganesa 10 Bandung 40132, Indonesia

ARTICLE INFO

Article history:
Received 28 April 2009
Received in revised form
27 July 2009
Accepted 9 August 2009
Available online 13 August 2009

Keywords:
Electrospinning
Nanofibers
Scaling laws

ABSTRACT

The development of various morphologies such as beads, beaded fibers, pure fibers and their scaling as a function of solution properties and processing variables in electrospinning is reported. Polyvinyl pyrrolidone (PVP), at various molecular weights and concentrations dissolved in a mixture of water and ethanol, was used to prepare different morphologies and sizes. The morphology of beads and fibers was predicted and measured based on an entanglement number diagram and rheological measurements. A constant-current electrospinning system was employed to control the processing variables. Scaling laws related to solution properties and processing variables (voltage, current and flow rate), and their effect on the fiber/bead diameter, were discussed. Viscosity (η), flow rate (Q), and current (I) were found to play significant roles in the control of morphology during electrospinning. Processing variables involved in electrospinning followed a power scaling that was in agreement with the model. The dependence of fiber diameter (d_f) on the Q/I for different molecular weights and concentrations also followed a power law, and the scaling varied between 0.11–0.29 for beaded fiber and 0.36–0.51 for pure fiber. In addition, the relationship between viscosity and fiber diameter followed scaling laws: $d_f \sim \eta^{0.98}$.

1. Introduction

Electrospinning provides a simple and versatile method for the generation of ultrathin fibers from a rich variety of materials that includes polymers, composites and ceramics [1]. Recently, electrospun fibers have attracted great attention due to their potential applications in tissue engineering scaffolds [2], filtration membranes [3], composite fibers [4], transparent conductive nanofibers [5,6], phosphorous [7,8], biocatalysts [9], etc. Driven by the widespread interest in nanofiber applications, a considerable amount of research has aimed to gain a better understanding of the electrospinning process, which is a potential process for the preparation of polymer fibers with diameters ranging from micro to nanometer scale, depending on the spinning conditions [10].

The electrospinning method is a variation of the electrospraying process. Both of these methods use high voltage to induce the formation of a liquid jet. In electrospraying, a solution of low viscosity is used to create an electrified jet that forms small droplets upon varicose break-up. In electrospinning, a highly viscous polymer solution is used to create the electrified jet, which is continuously stretched by electrostatic repulsions between the surface charges and the evaporation solvent, forming a solid fiber [1]. The morphology of electrospun polymer ranges from particles (electrospray) to pure fibers, depending on various conditions. Three main issues are involved in attempting to obtain the desirable morphologies: solution properties, environmental conditions, and processing variables [10,11]. The solution properties are viscosity, conductivity, surface tension, etc. The operating parameters are flow rate, jet current, applied potential and distance between the spinneret and the collector. The evaporation rate of the solvent, as a function of environmental conditions, is also known to affect the final diameter of the fibers [12]. Solution properties are determined before the electrospinning process, while environmental conditions are usually fixed to diminish the influence of changes in the evaporation rate on fiber solidification. Therefore, only processing variables can control the morphology of the fiber during the electrospinning process.

In order to predict the resulting morphology for a given condition, the contribution of solution properties, environmental conditions and processing variables must be considered. A number of publications have been reported on the effect of electrospinning conditions on the resulting fiber morphology. However, comprehensive studies on the development of various morphologies of electrospinning products and their scaling laws have rarely been reported. The purpose of this article is to spotlight the development of various morphologies such as beads, beaded fibers, pure fibers, and their scaling, as a function of solution properties and processing variables using a constant-current electrospinning system [13,14]. Polyvinyl pyrrolidone (PVP) concentrations, at different

* Corresponding author.
E-mail address: okuyama@hiroshima-u.ac.jp (K. Okuyama).

0032-3861/$ – see front matter © 2009 Elsevier Ltd. All rights reserved.
doi:10.1016/j.polymer.2009.08.011

Nomenclature

$(n_e)_{soln}$	entanglement number (dimensionless)	κ	the dielectric constant of the solution ($A^2s^4\,kg^{-1}\,m^{-3}$)
M_w	molecular weight ($kg\,k\,mol^{-1}$)	ε_0	the permittivity of a vacuum ($A^2s^4\,kg^{-1}\,m^{-3}$)
M_e	entanglement molecular weight ($kg\,k\,mol^{-1}$)	Q	flow rate ($l\,min^{-1}$)
ϕ	volume fraction (dimensionless)	K	electrical conductivity ($S\,m^{-1}$)
$C\sim$	the characteristic ratio	γ	the surface tension ($N\,m^{-1}$)
m_o	the average molecular weight per backbone bond ($kg\,k\,mol^{-1}$)	h_r	the jet radius (m)
		h_t	the jet diameter (m)
l_o	bond length (m)	I	electric current (A)
ρ	density ($kg\,m^{-3}$)	E	voltage (V)
D_{drop}	the predicted diameter of the droplet (m)	d	fiber diameter (m)
		c	concentration (dimensionless)
		η	viscosity (cp)

molecular weights, required to prepare different morphologies (pure beads, beaded fiber and pure fiber), were calculated and measured based on an entanglement number diagram and rheological measurements. In order to produce uniform and controllable morphology with high reproducibility, a constant-current electrospinning system was employed to control the processing variables. Some scaling laws related to solution properties and processing variables (voltage, current and flow rate) and their effect on the fibers/beads diameter were discussed.

2. Experimental

The hardware configuration of the electrospinning system was similar to that described in the authors' previous studies [13,14]. A precursor solution was placed in a hypodermic syringe at a fixed distance (10 cm) from the cathode (an aluminum plate with 10 cm in diameter) is used to collect produced fibers. The positive terminal (anode, an aluminum plate with 10 cm in diameter) of a variable high voltage source (HVS) (Matsusada HER 20R3), which was capable of delivering a dc voltage up to 20 kV, was attached to the precursor solution in the hypodermic syringe equipped with a syringe pump (Harvard Apparatus PHD 2000). The cathode was covered by aluminum foil where the fibers were deposited. The electric current in the electrospinning process was determined by a resistor, R, in series between the collector and the ground. In order to quantify instantaneous current in the electrospinning system, the voltage drop across the resistor was measured in real-time by using an analog to a digital system (Contec AI-1608AY-USB), in which a universal serial bus (USB) communication was provided to send the digital output to a computer. The electric current flowing through the region between the electrodes was measured and kept at a certain value by adjusting the voltage applied to the electrodes. For the purpose of keeping at a certain value of the current during the electrospinning process, a proportional-integral-derivative (PID) control action was applied to the electrospinning system.

Polyvinyl pyrrolidone (PVP, Sigma–Aldrich, Saint Louis, MO, USA) with four different molecular weights (M_w), 10 k, 29 k, 55 k and 350 k, were used in this study. To prepare solutions with different weight percent concentrations, weighted amounts of polymers and solvents (1:1 mixture of deionized water and ethanol by volume) were mixed and stirred for several hours until homogeneous solutions were obtained. Surface tension measurements were made using an automatic surface tensiometer (CBVP-2, Kyowa Interface Science Co., Ltd.). Dynamic viscosity measurements were made using a Brookfield DV-III rheometer (Brookfield, Middleboro, MA, USA) and solution electrical conductivities were measured using a TCX-90i conductivity meter (Toko Chemical Laboratories Co., Ltd., Japan). Scanning electron microscopy (SEM) images of the samples were obtained using field emission scanning electronic microscopy (FE-SEM, S-5000, Hitachi Corp., Tokyo, Japan). The precursor solution was drawn using a 1-ml syringe mounted horizontally on the syringe pump. The environment during the electrospinning process was kept at a temperature of $(32 \pm 2)\,^{\circ}C$ and a relative humidity (RH) of $(45 \pm 5)\%$.

3. Results and discussion

3.1. Constant-current electrospinning system performance

In order to produce uniform nanofibers with high reproducibility, it is necessary to maintain the stability of the cone jet corresponding to the stability of the constant current. Some papers have reported that the electric current affected the resulting fiber morphology during electrospinning [15,16]. The shape of the jet and morphology of the fiber corresponded to the stability of the current [13,17]. Fig. 1 shows that the electric current in the cone jet mode (inset Fig. 1) was very stable during the electrospinning process. The applied voltage was controlled and changed slightly to maintain a constant desirable current. Another inset in Fig. 1 shows that the constant-current electrospinning system was resistant to disturbance caused by various factors such as changes in the surface tension and the viscosity of the precursor solution. The desired electric current was restored in less than 2 s following a disturbance occurring for 0.5 s. It is believed that this rapid restoration will not perturb the production of uniform nanofibers [13,14]. All experiments in this study were performed in a stable cone-jet mode and in a constant desirable current.

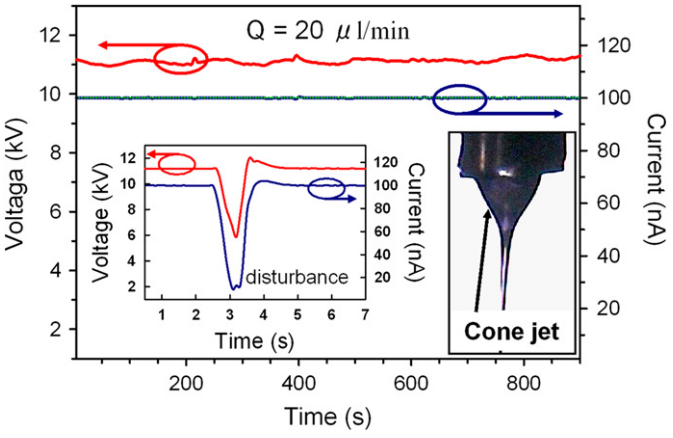

Fig. 1. Relationship between the electric current and time for M_w, concentration and flow rate of 350 k, 15 wt% and 20 μl/min, respectively.

Table 1
Properties of polymer solutions.

M_w (kg/mol)	Concentration ϕ (wt%)	Viscosity η (cp)	Conductivity κ (μS/cm)	Surface tension σ (N/m)
10	10	6.0	140.0	0.029
10	20	8.6	214.3	0.029
10	30	17.4	225.3	0.031
10	40	44.7	202.7	0.033
29	20	18.5	70.2	0.030
29	30	54.2	76.3	0.031
29	35	92.7	74.8	0.032
29	40	153.4	69.8	0.033
55	20	32.2	47.6	0.030
55	25	56.0	49.6	0.030
55	30	101.5	49.7	0.031
55	35	177.9	47.6	0.031
55	40	312.1	46.6	0.032
350	3	16.7	5.4	0.029
350	6	56.3	9.0	0.029
350	9	147.8	11.4	0.030
350	12	353.8	14.4	0.030
350	15	752.6	16.7	0.030

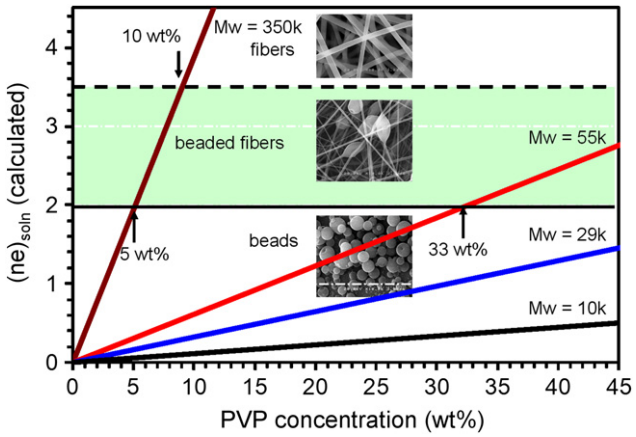

Fig. 2. Plot of the calculated entanglement number $(n_e)_{soln}$ as a function of concentration for PVP/(water/ethanol) systems for various molecular weights. The dashed line indicates the transition for complete fiber formation, while the solid line indicates the boundary between beads and a mixture of fibers and beads.

3.2. Effects of solution properties on bead and fiber morphology

Resistance to jet breakup in cone-jets of many polymer solutions has been correlated with the number of polymer entanglements (overlaps between polymer chains) in the solution (Table 1). Shenoy et al. [18,19] have developed a semi-empirical theory, in which the critical parameter determining the "electrospinnability" of a solution is the entanglement number, $(n_e)_{soln}$, defined as

$$(n_e)_{soln} = \frac{\phi M_w}{M_e} \quad (1)$$

M_w is the molecular weight of the polymer in the solution and M_e is the polymer entanglement molecular weight, which is a function of polymer chain topology and morphology [18]. An entanglement number of 2 for a polymer solution corresponds to approximately 1 entanglement per chain, and for pure fiber formation by electrospinning, it is typically necessary to use a polymer solution with an entanglement number greater than 3.5. At an entanglement number between 2 and 3.5, there will be a transition from beaded fiber to pure fiber. At an entanglement number less than 2, there will be a pure electrospray process that produces pure particles. In this study, the estimated value of $M_{e(PVP)}$ was determined using the entanglement constraint model [20]

$$M_e \propto C_\infty^{-3} m_0^3 l_0^{-6} \rho^{-2} \quad (2)$$

where C_∞, m_o, l_o and ρ are the characteristic ratios, the average molecular weight per backbone bond, bond length, and density, respectively. Using the relationship above, the value of $M_{e(PVP)}$ can be estimated by comparing with a reference polymer possessing a similar topological structure. Polystyrene (PS) was chosen as the reference, thereby eliminating l_o as a variable (since $l_o(PS) = l_o(PVP)$), and the calculated value of C_∞ (PVP/ethanol–water) was 12.3 [18]. Employing an $M_{e(PS)}$ of 16.6 k and a correction of $(M_e \times 5/4)$, as found in the literature, [18] $M_{e(PVP)}$ was estimated, using equation (2), to be 12.3 k.

Fig. 2 shows plots of the calculated $(n_e)_{soln}$ as a function of PVP concentration for different molecular weights (10–350 kg/mol). Focusing on the 350 k plot, three distinct morphology regimes are shown: pure beads, beaded fibers and pure fibers. Below 5 wt%, $(n_e)_{soln} \sim 2$, only beaded morphology was predicted. With increasing concentration above $(n_e)_{soln} \sim 2$, beaded fiber and a mixture of fiber + beads were predicted. When the PVP concentration was increased to 10 wt%, pure fibers were predicted, which corresponds to $(n_e)_{soln} \sim 3.5$ (2.5 entanglements/chain). In the 55 k plot, only two regimes were predicted: pure beads and beaded fibers. Below $(n_e)_{soln} \sim 2$ (33 wt%), pure beads were predicted, while above 33 wt% beaded fibers were predicted. In addition, for 29 k and 10 k only pure beads were predicted for concentrations up to 45 wt%.

Fig. 3 shows different structural regimes during the bead-fiber transition for various molecular weights and concentrations. For $M_w = 350$ kg/mol, morphological variation of beads, including beaded fiber and pure fiber, was observed, and this agreed very well with the prediction in Fig. 2. For concentrations below $(n_e)_{soln} \sim 2$, which was estimated to be 5 wt%, structures consisting only of beads were obtained [Fig. 3(a)]. When the concentration was increased to $(n_e)_{soln} \sim 2$ and above, structures of beaded fiber were obtained [Fig. 3(b)]. Moreover, structures of pure fiber were obtained for $(n_e)_{soln} > 3.5$, which corresponds to the concentration of 12 wt% [Fig. 3(c)]. However, we observed discrepancies between the predictions and the observations for M_w of 55, 29 and 10 kg/mol. The reduction in polymer molecular weight significantly affected the level of increase in the concentration at which morphological transitions took place. The beaded fibers were obtained at concentrations as high as 25, 30 and 40 wt% for molecular weights of 55, 29 and 10 k, respectively. Pure fibers began to form only for M_ws of 55 and 29 kg/mol at concentrations of 35 and 40 wt%, respectively. A similar result was reported by Eda et al. [21]. The formation of fibers in low-molecular weight solutions may be attributed to the rapid solidification of the jet. For concentrated solutions, evaporation of a small amount of solvent may lead to immediate skin formation. The speculation is that the solution jet ejected from the Taylor cone undergoes solidification, before Rayleigh instability can take effect [21]. The entanglement analysis was a good predictor for PVPs of high molecular weight, but less for those of low molecular weight. There are other factors that can influence fiber formation, the two most important being the electric field and surface tension, which affect both the Taylor cone and fiber/bead formation [18].

A plot of the viscosity as a function of concentration for various molecular weights is shown in Fig. 4. Within the range of concentrations investigated, distinct variation in the slopes with concentration was observed. The different morphologies resulting from electrospray/electrospinning were found to depend strongly on the

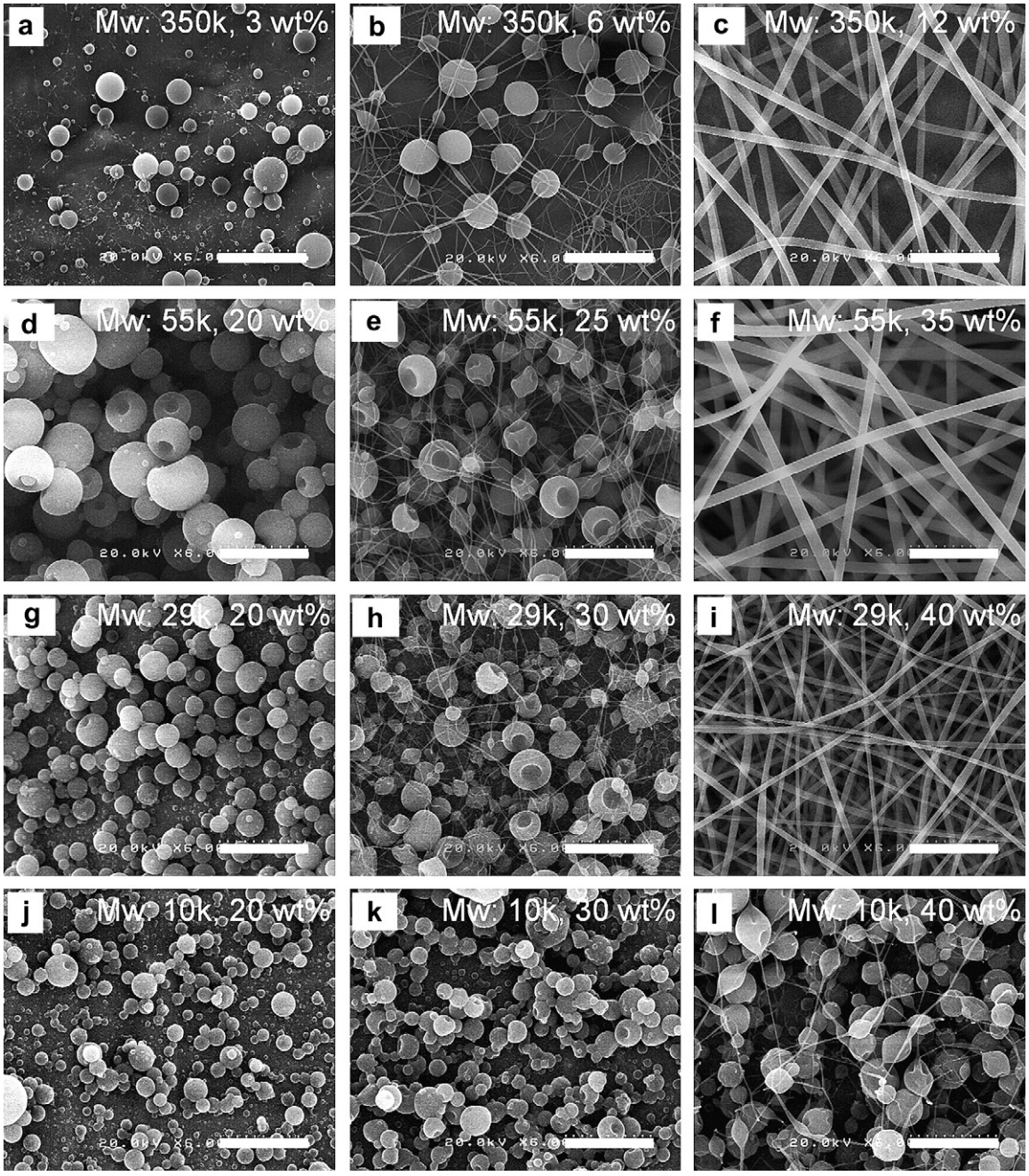

Fig. 3. SEM photographs showing different structural regimes during bead-fiber transition at a flow rate of 8 μl/min, for various molecular weights and concentrations.

solution viscosity. The formation of a pure bead, beaded fiber and pure fiber was relatively similar for all molecular weights, due to the solution viscosity. The transition regime between pure bead and beaded fiber (dotted line) was observed at a viscosity of ~40 cp for all molecular weights. Furthermore, a pure fiber regime was obtained at viscosities higher than ~160 cp (dashed line). These transition regimes may differ for different polymer solutions. Mc Kee et al. reported that these transition regimes occurred at solution viscosities of 10 and 30 cp for polyester solutions [11]. The cross label is a graphic representation of the dependence of specific viscosity (η_{sp}) on concentration according to Mc Kee et al. [11] for a M_w of 350 kg/mol. The specific viscosity was defined as follows: (zero shear viscosity – solvent viscosity)/solvent viscosity. The slopes in the high concentration regimes were estimated to be 3.9, which is in agreement with the theoretical scaling law exponent and experimental investigation by Mc Kee et al. [11]

3.3. Effects of processing variables on bead and fiber morphology

Solution concentration reportedly has a significant effect on the final size and distribution of particles in the electrospraying process. In electrospinning, solution viscosity and surface tension also play important roles in determining the range of concentrations from which continuous fibers can be obtained. For low viscosity solutions, several scaling laws, which relate process parameters and solution properties to the size of the droplets produced by electrospray, have been developed. Rosell-Llompart and Fernandez de la Mora [22], as well as Chen and Pui [23],

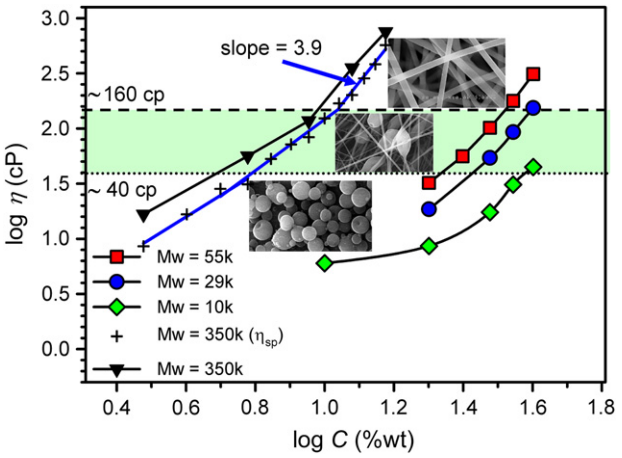

Fig. 4. Plot of the viscosity as a function of concentration for various molecular weights. The dashed line indicates the transition for complete fiber formation, while the dotted line indicates the boundary between beads and a mixture of fibers and beads (obtained from the experiment).

developed a semi-empirical model to predict the initial droplet size for electrospray in the cone-jet mode:

$$D_{\text{drop}} = G(\kappa)\left(\kappa\varepsilon_0\frac{Q}{K}\right)^{1/3} \tag{3}$$

D_{drop} is the predicted diameter of the droplet, κ the dielectric constant of the solution, ε_0 the permittivity of a vacuum, Q the solution flow rate, K the solution electrical conductivity, and $G(\kappa)$ is given by [23]:

$$G(\kappa) = -10.9\kappa^{-6/5} + 4.08\kappa^{-1/3} \tag{4}$$

Therefore, the particle diameter is a function of solution flow rate that follows power scaling.

Fig. 5 (a–c) shows the SEM images of particles produced by different flow rates for low viscosity. It appears that particle diameter increased as flow rate increased, which is in agreement with the model [22,23]. Fig. 5(d–f) shows the pure fiber morphology obtained from electrospinning of high viscosity solutions. Smooth and uniform fibers were obtained due to the stability of the cone-jet, corresponding to the stability of the desired constant-current. Fiber diameter increased as flow rate increased, in agreement with previous observations [6,24]. For medium viscosity solutions, beaded morphology was obtained and could be controlled by controlling the processing variables [Fig. (g–i)]. Beaded fibers were observed widely in the electrospinning process, and were considered as a demerit of the electrospun fibers. However, in some applications, for example for the development of high performance filter media [25], control of the bead morphology must be considered. There are many factors affecting the occurrence of beads, such as applied voltage, viscoelasticity of the solution, charge density and surface tension of the solution. In this study, the number and morphology of beaded fibers could be easily

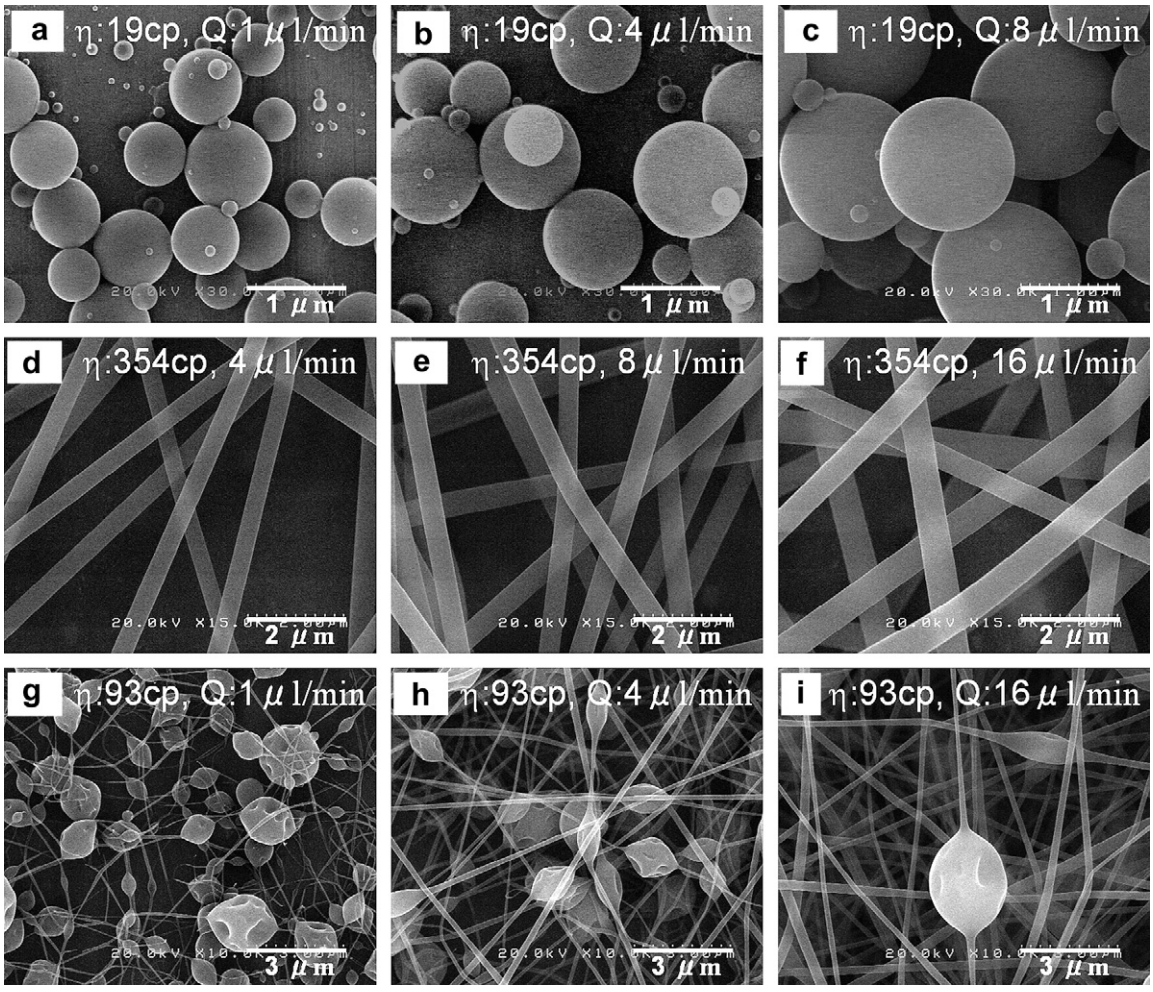

Fig. 5. SEM photographs showing the effect of flow rate on the beads, beaded fiber and fiber morphology for a given viscosity.

controlled by adjusting the flow rate in cone-jet mode. It was found that the beaded and fiber diameters increased as the flow rate increased. However, the number of beads was reduced as the flow rate increased.

Many researchers have reported that beaded morphology could be controlled by controlling solution properties. For example, a solution with a high charge density results in a fine fiber structure, due to the large extensional force in a jet of solution [21]. Moreover, the use of solvents with a large dielectric constant and electrical conductivity typically results in increased uniformity and a reduced number of beads [26–28]. The effects of processing variables on beaded morphology have rarely been reported, although controlling these is easier and more cost-effective than controlling solution properties. Lee et al. demonstrated that bead morphology changed with different applied voltages [27]. Fig. 6 shows morphology change in the electrospinning product by controlling the flow rate. In cone-jet mode, it was found that the morphology of the product could be controlled, from pure beads to beaded fiber, by adjusting the flow rate.

3.4. Scaling for processing variables during electrospraying and electrospinning

In order to facilitate the use of a cone-jet mode in electrospinning and electrospray, an understanding of the basic scaling of processing variables is required. Several researchers have reported scaling laws for processing variables (electric current, voltage, flow rate) involved during electrospinning/electrospraying in the cone-jet mode. Ganan-Calvo et al. reported that the current flow rate scaling relationships were divided into two distinguished limits of liquid physical properties [29]:

a. Sufficiently high liquid viscosity:

$$I = 2.4(QK\gamma)^{1/2} \tag{5}$$

b. Low liquid viscosity:

$$I = 8.6\left(\frac{QK\varepsilon_0\gamma^3}{\rho}\right)^{1/4}, \tag{6}$$

where γ is the surface tension. This analysis is based on the assumption that the close-up electric field acting on the microjet is due to the exact conical solution, owing to Taylor.

He et al. developed a scaling relationship between current and flow rate, which can be expressed as [30]:

$$I \sim Q^{\frac{2(\delta+1)}{\alpha(2\delta+1)}} \tag{7}$$

The value of parameter δ depends upon conductivity and polymer concentration. He et al. also reported the allometric scaling relationship between current and voltage as [31]:

$$I \sim E^{\frac{a(2\delta+1)}{a(2\delta+1)-2(\delta+1)}} \tag{8}$$

Therefore, in electrospinning and electrospraying the scaling relationship between current-flow rate and current-voltage can be simplified as power law $I \sim Q^{\alpha}$ and $I \sim E^{\beta}$, respectively. In this case, α and β are constants that depend on the solution properties and environmental conditions.

Fig. 7 shows the relationship between voltage and current for PVP with different molecular weights, concentrations and flow rates. It can be observed that in similar M_w, current–voltage relationships do not change significantly for different concentrations. The resulting measurements exhibit a power law dependence between current and voltage with different power scaling (α) for different molecular weights. The power scaling varies from 3.1 to 3.5 for molecular weights of 350–29 kg/mol. Similar results were also reported for polycaprolactone (PCL) and polyurethane (PU) solutions [31,32]. Theron et al. [33] working with PU, PCL, polyethylene oxide (PEO), polyvinyl alcohol, and polyacrylic acid (PAA) solutions reported that the power-law relationship between voltage and current with an exponent value varies between 2.166 and 4.565.

The relationship between log flow rate and log current in cone-jet mode for PVP with different molecular weights, concentrations

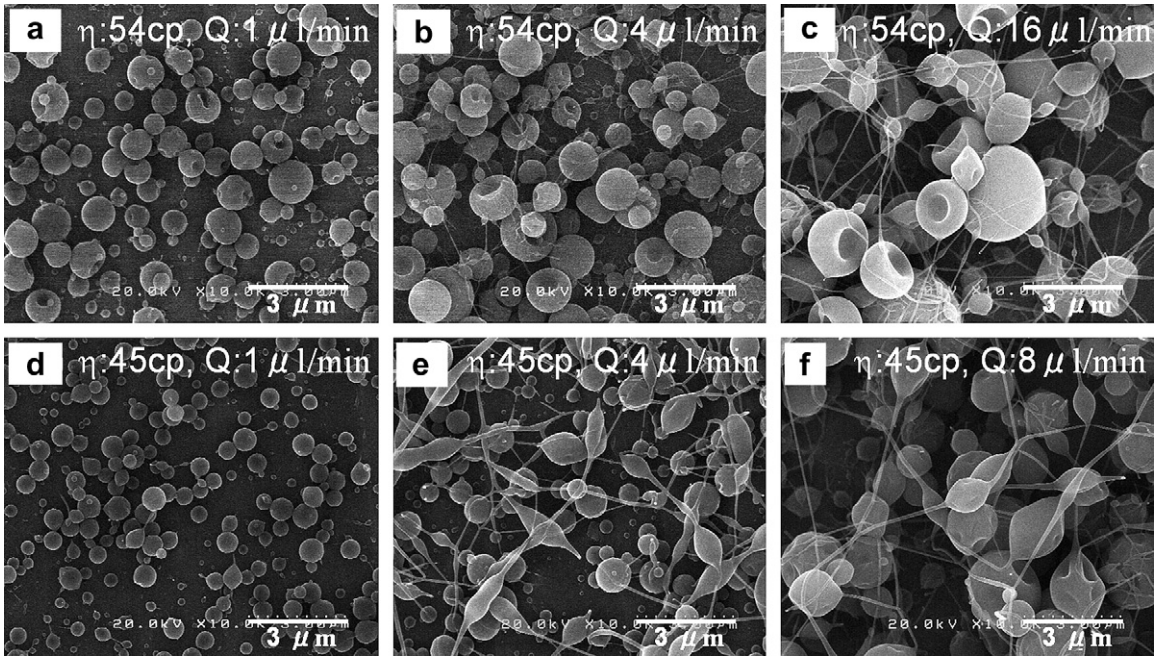

Fig. 6. SEM photographs showing the effect of flow rate on the transition control of the beads and beaded fibers for a given viscosity.

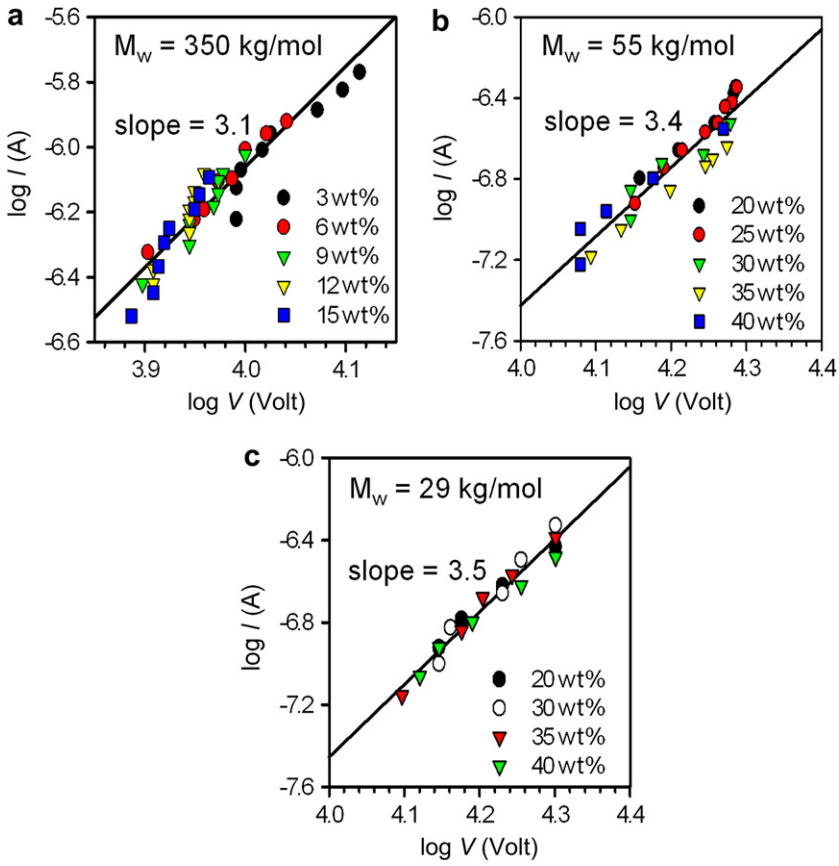

Fig. 7. The scaling relationship between voltage and current for PVP at different concentrations and flow rates for molecular weights of (a) 350, (b) 55 and (c) 29 kg/mol.

and flow rates is shown in Fig. 8. The slope and intercept changes slightly for different concentrations in similar M_w. The slopes for different molecular weights also change slightly in the range 0.48–0.64. These results also exhibit a power-law dependence between flow rate and current, which is in agreement with the model and previous observations [29,30,32]. Theron et al. also reported a power-law relationship between I and Q with different exponent values for different solutions [33].

3.5. Scaling for bead and fiber diameter

One of the most important quantities related to electrospinning is the fiber diameter [34]. When the fiber diameter is decreased from 100 μm to 100 nm, the specific surface area of the fibers increases 1000-fold. This translates to greater efficiency and a reduction in the weight of required materials, without altering the surface area in fibers with smaller diameters (increasing the specific surface area). These properties make nanofiber-based materials optimally suited for many important applications, such as photo-catalysts and filtration devices. Many researchers have developed an analytical model relating the effect of electrospinning parameters on the jet/fiber diameter. Spivak et al. developed an electro-hydro-dynamic model of steady-state electrospinning in a single jet regime [35]. The nonlinear rheologic constitutive equation (Oswald–deWaele law) was used to describe polymer fluids. The model prediction for jet radius is:

$$h_r = 2[\varepsilon_0\gamma]^{1/3}\left(\frac{Q}{I}\right)^{2/3} \tag{9}$$

where h_r is the jet radius. Fridrikh et al. presented a model of a charged fluid jet in an electric field under conditions applicable to whipping instability [16]. The model predicts a terminal jet diameter, which is a consequence of balance between normal stresses due to surface tension and surface charge repulsion, and can be determined from knowledge of the flow rate, electric current, and the surface tension of the fluid [16]. The terminal jet diameter was predicted using an equation that resembles equation (9), as follows:

$$h_t = \left[\gamma\varepsilon\frac{2}{\pi(2\ln\chi - 3)}\frac{Q^2}{I^2}\right]^{1/3} \tag{10}$$

Here, h_t is the jet diameter and $\chi \approx R/h$, where R is the radius of the curvature. Assuming that solvent evaporation is insignificant prior to the attainment of the limiting jet diameter, and that evaporation changes the diameter but not the length of the thread, Fridrikh et al. estimated the fluid jet diameter that gives rise to a solid fiber diameter (d) by correcting the polymer concentration (c): $h_t = d/c^{0.5}$. From equations (9) and (10), it can be concluded that jet/fiber diameter depends on the solution properties (surface tension) and processing variables (flow rate and current).

Fig. 9 shows a plot of log Q/I against log d_f (average fiber diameter) for different molecular weights and concentrations. Fibers containing beads are smaller than pure fibers, which is due to capillary breakup. It can be observed that the relationship follows a power-law for both pure fibers and beaded fibers. However, the power scaling varies between 0.11–0.29 for beaded fibers and 0.36–0.51 for pure fibers. This difference in power scaling may depend on the solution properties (viscosity). The model developed by Fridrikh et al. [16] neglected the effects of viscosity and conductivity on final fiber diameter. Between the nozzle regime and the asymptotic regime, viscosity may play a role in determining the rate of jet thinning [36].

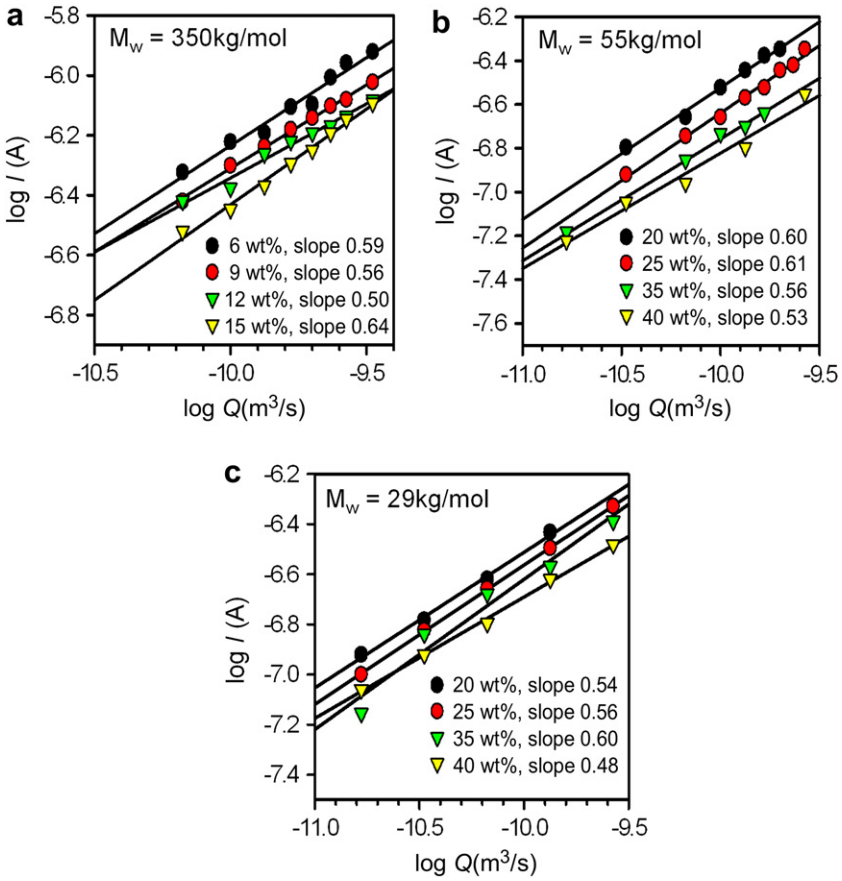

Fig. 8. The scaling relationship between flow rate and current f for PVP with different concentrations and flow rates for molecular weights of (a) 350, (b) 55 and (c) 29 kg/mol.

In order to confirm the viscosity dependence on the average fiber diameter, viscosity was plotted against average fiber diameter for different processing variables (flow rates), as shown in Fig. 10. The linear regression on the data corresponding to log viscosity (η) – log average fiber diameter (d_f) gave: $d_f \sim \eta^{0.98}$. Fiber diameter was strongly dependent on the viscosity with a power scaling of 0.98. An increase in the solution viscosity indicated a larger number of entanglement couplings, thereby generating larger electrospun fibers. It has been reported that different scaling exponents may apply for polymer solutions with different rheological properties.[10,37] Hence, the extensional viscosity of the jet, while in flight to the target, is undoubtedly very influential in governing the stretching induced in the jet, which in turn affects the final diameter of the fiber. The inset in Fig. 10 shows the relationship of the fiber diameter d_f and the flow rate Q for different viscosities. A clear trend was observed wherein the fiber diameter increased as the increment of the flow rate followed a power scaling with the intercept, which increased as the viscosity increased.

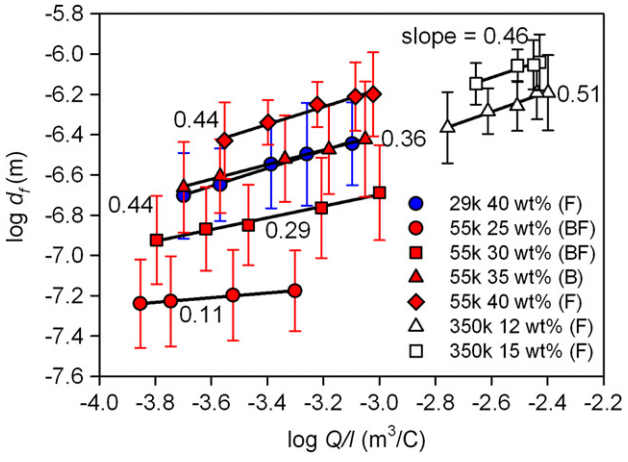

Fig. 9. Average fiber diameter as a function of Q/I (the inverse of volume charge density) for various molecular weights and concentrations. BF: beaded fiber, F: fiber.

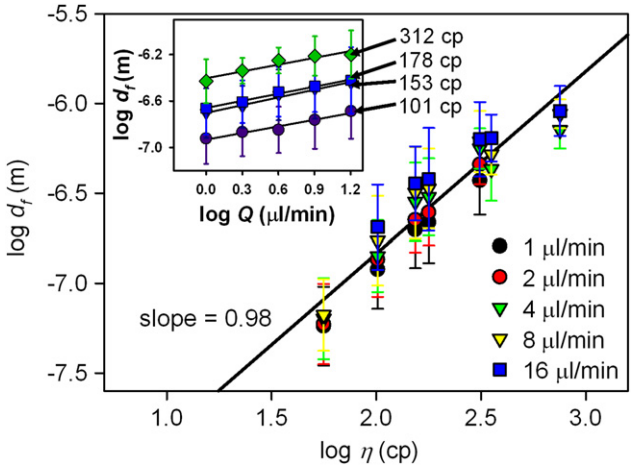

Fig. 10. Solution viscosity effects on average fiber diameter d_f for various molecular weights and concentrations.

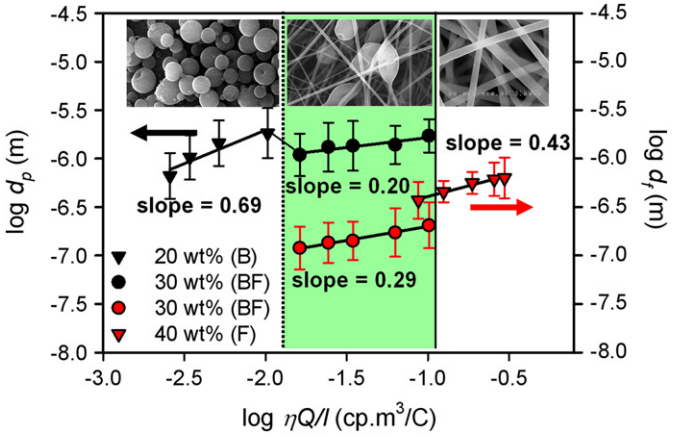

Fig. 11. Average bead and fiber diameters as a function of viscosity and Q/I (the inverse of volume charge density) for a molecular weight of 55 kg/mol. The solid line indicates the transition to complete fiber formation, while the dotted line indicates the boundary between beads and a mixture of fibers and beads.

A plot of the average bead and fiber diameter as a function of viscosity and Q/I (the inverse of volume charge density) for a molecular weight of 55 kg/mol is shown in Fig. 11. The solid line indicates the transition to complete fiber formation, while the dotted line indicates the boundary between beads and beaded fibers. From this figure, it is clear that bead, beaded fiber and pure fiber formation was mainly controlled by viscosity and processing variables (flow rate and electric current). The slopes of pure fiber (0.43), as well as pure beads (0.69), were higher than that of beaded fiber. The changes of morphology and its scaling were clearly shown using this relationship. The morphology was mainly controlled by viscosity; meanwhile, the bead/fiber diameter and its transition during the electrospinning process were controlled by the processing variables (flow rate and current). The transition regime, as shown in Fig. 11, would merely be shifted for different polymer solutions, but would have the same trend and behavior.

4. Conclusions

The authors have developed various morphologies such as beads, beaded fibers, and pure fibers, and their scaling as a function of solution properties and processing variables, by electrospinning of PVP at various molecular weights and concentrations dissolved in a mixture of water and ethanol. The entanglement analysis shows a good prediction of fiber/bead formation for PVP with high molecular weight, and less success with low molecular weight. The solution viscosity plays a significant role in bead/fiber formation. The transition regimes occurred at solution viscosities of 40 and 160 cp for all PVP solutions. During the electrospinning process, the flow rate and current controls the resulting morphology. The scaling relationship between current-flow rate and current-voltage follows power laws $I \sim Q^{\alpha}$ and $I \sim E^{\beta}$, respectively. The constant α varies from 3.1 to 3.5 for M_w of 350 to 29 kg/mol and β in the range of 0.48–0.64, which is in agreement with the model and previous observations. The relationship between Q/I and fiber diameter also follows a power law for both pure fiber and beaded fiber. Moreover, viscosity plays a significant role in the final fiber diameter with the power scaling of 0.98.

Acknowledgements

This work was supported by a Grant-in-Aid for Scientific Research (A) 18206079 from the Japan Society for the Promotion of Science (JSPS). We gratefully acknowledge the Ministry of Education, Culture, Sports, Science and Technology (MEXT) of Japan for the provision of a doctoral scholarship (M.M.M.)

References

[1] Li D, Xia YN. Adv Mater 2004;16:1151.
[2] Wnek GE, Carr ME, Simpson DG, Bowlin GL. Nano Lett 2003;3:213.
[3] Yun KM, Hogan CJ, Matsubayashi Y, Kawabe M, Iskandar F, Okuyama K. Chem Eng Sci 2007;62:4751.
[4] Liu ZY, Sun DDL, Guo P, Leckie JO. Nano Lett 2007;7:1081.
[5] Munir MM, Widiyandari H, Iskandar F, Okuyama K. Nanotechnology 2008;19:375601.
[6] Munir MM, Iskandar F, Yun KM, Okuyama K, Abdullah M. Nanotechnology 2008;19:145603.
[7] Munir MM, Yun KM, Iskandar F, Yabuki A, Okuyama Y. Jpn J Appl Phys Part 1 2007;46:6705.
[8] Suryamas AB, Munir MM, Iskandar F, Okuyama Y. J Appl Phys 2009;105:064311.
[9] Jia HF, Zhu GY, Vugrinovich B, Kataphinan W, Reneker DH, Wang P. Biotechnol Prog 2002;18:1027.
[10] Wang C, Hsu CH, Lin JH. Macromolecules 2006;39:7662.
[11] McKee MG, Wilkes GL, Colby RH, Long TE. Macromolecules 2004;37:1760.
[12] Tripatanasuwan S, Zhong ZX, Reneker DH. Polymer 2007;48:5742.
[13] Munir MM, Iskandar F, Khairurrijal, Okuyama K. Rev Sci Instrum 2008; 79:093904.
[14] Munir MM, Iskandar F, Khairurrijal, Okuyama K. Rev Sci Instrum 2009; 80:026106.
[15] Kim SJ, Shin KM, Kim SI. Scripta Mater 2004;51:31.
[16] Fridrikh SV, Yu JH, Brenner MP, Rutledge GC. Phys Rev Lett 2003;90:144502.
[17] Samatham R, Kim KJ. Polym Eng Sci 2006;46:954.
[18] Shenoy SL, Bates WD, Frisch HL, Wnek GE. Polymer 2005;46:3372.
[19] Shenoy SL, Bates WD, Wnek G. Polymer 2005;46:8990.
[20] Fetters LJ, Lohse DJ, Richter D, Witten TA, Zirkel A. Macromolecules 1994; 27:4639.
[21] Eda G, Shivkumar S. J Appl Polym Sci 2007;106:475.
[22] Roselllompart J, Delamora JF. J Aerosol Sci 1994;25:1093.
[23] Chen DR, Pui DYH. Aerosol Sci Technol 1997;27:367.
[24] Wang T, Kumar S. J Appl Polym Sci 2006;102:1023.
[25] Kalayci V, Ouyang M, Graham K. Filtration 2006;6:286.
[26] Lee KH, Kim HY, La YM, Lee DR, Sung NH. J Polym Sci Part B Polym Phys 2002; 40:2259.
[27] Lee KH, Kim HY, Bang HJ, Jung YH, Lee SG. Polymer 2003;44:4029.
[28] Eda G, Liu J, Shivkumar S. Eur Polym J 2007;43:1154.
[29] Ganan-Calvo AM, Barrero A. J Aerosol Sci 1996;27:S179.
[30] He TH, Wan YQ, Yu JY. Polymer 2005;46:2799.
[31] He JH, Wane YQ. Polymer 2004;45:6731.
[32] Demir MM, Yilgor I, Yilgor E, Erman B. Polymer 2002;43:3303.
[33] Theron SA, Zussman E, Yarin AL. Polymer 2004;45:2017.
[34] Huang ZM, Zhang YZ, Kotaki M, Ramakrishna S. Compos Sci Technol 2003;63:2223.
[35] Spivak AF, Dzenis YA, Reneker DH. Mech Res Commun 2000;27:37.
[36] Rutledge GC, Fridrikh SV. Adv Drug Deliv Rev 2007;59:1384.
[37] Wang C, Hsu CH, Hwang IH. Polymer 2008;49:4188.